Protein Structure and Folding:

A Positive Cooperativity Binding Model between Ly49 Natural Killer Cell Receptors and the Viral Immunoevasin m157: KINETIC AND THERMODYNAMIC STUDIES

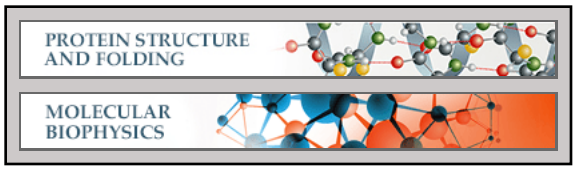

Pablo N. Romasanta, Lucrecia M. Curto, Nicolas Urtasun, María B. Sarratea, Santiago Chiappini, María V. Miranda, José M. Delfino, Roy A. Mariuzza, Marisa M. Fernández and Emilio L. Malchiodi

J. Biol. Chem. 2014, 289:5083-5096.
doi: 10.1074/jbc.M113.532929 originally published online December 30, 2013

THE JOURNAL OF BIOLOGICAL CHEMISTRY VOL. 289, NO. 8, pp. 5083–5096, February 21, 2014

A Positive Cooperativity Binding Model between Ly49 Natural Killer Cell Receptors and the Viral Immunoevasin m157

KINETIC AND THERMODYNAMIC STUDIES[*S]

Received for publication, November 6, 2013, and in revised form, December 11, 2013 Published, JBC Papers in Press, December 30, 2013, DOI 10.1074/jbc.M113.532929

Pablo N. Romasanta[‡], Lucrecia M. Curto[§], Nicolas Urtasun[¶], María B. Sarratea[‡], Santiago Chiappini[‡], María V. Miranda[¶], José M. Delfino[§], Roy A. Mariuzza[‖], Marisa M. Fernández[‡], and Emilio L. Malchiodi[‡1]

From the [‡]Cátedra de Inmunología and Instituto de Estudios de la Inmunidad Humoral (IDEHU), Consejo Nacional de Investigaciones Científicas y técnicas - Universidad de Buenos Aires (CONICET-UBA) and [¶]Cátedra de Microbiología Industrial y Biotecnología, Facultad de Farmacia y Bioquímica, Universidad de Buenos Aires, Buenos Aires C1113AAD, Argentina, [§]Departamento de Química Biológica and Instituto de Química y Fisicoquímica Biológica (IQUIFIB), CONICET-UBA, Facultad de Farmacia y Bioquímica, Universidad de Buenos Aires, Buenos Aires C1121ABG, Argentina, and [‖]W. M. Keck Laboratory for Structural Biology, University of Maryland Institute for Bioscience and Biotechnology Research, Rockville, Maryland 20850

Background: m157 is a cytomegalovirus immunoevasin that binds Ly49 natural killer cell receptors.
Results: Kinetic and thermodynamic analyses revealed the mechanism underlying the Ly49/m157 interaction.
Conclusion: The binding mechanism is characterized by positive cooperativity and conformational selection.
Significance: This mechanism provides a biophysical framework for interpreting crystal structures of Ly49 receptors.

Natural killer (NK) cells discriminate between healthy and virally infected or transformed cells using diverse surface receptors that are both activating and inhibitory. Among them, the homodimeric Ly49 NK receptors, which can adopt two distinct conformations (backfolded and extended), are of particular importance for detecting cells infected with mouse cytomegalovirus (CMV) via recognition of the viral immunoevasin m157. The interaction of m157 with activating (Ly49H) and inhibitory (Ly49I) receptors governs the spread of mouse CMV. We carried out kinetic and thermodynamic experiments to elucidate the Ly49/m157 binding mechanism. Combining surface plasmon resonance, fluorescence anisotropy, and circular dichroism (CD), we determined that the best model to describe both the Ly49H/m157 and Ly49I/m157 interactions is a conformational selection mechanism where only the extended conformation of Ly49 (Ly49*) is able to bind the first m157 ligand followed by binding of the Ly49*/m157 complex to the second m157. The interaction is characterized by strong positive cooperativity such that the second m157 binds the Ly49 homodimer with a 1000-fold higher sequential constant than the first m157 ($\sim 10^8$ *versus* $\sim 10^5$ M^{-1}). Using far-UV CD, we obtained evidence for a conformational change in Ly49 upon binding m157 that could explain the positive cooperativity. The rate-limiting step of the overall mechanism is a conformational transition in Ly49 from its backfolded to extended form. The global thermodynamic parameters from the initial state (backfolded Ly49 and m157) to the final state (Ly49*/$(m157)_2$) are characterized by an unfavorable enthalpy that is compensated by a favorable entropy, making the interaction spontaneous.

Natural killer (NK)[2] cells are essential components of the innate immune response against viral infections and tumors (1–3). The cytolytic activity of NK cells is regulated by a dynamic interplay between activating and inhibitory signals transmitted by distinct classes of receptors on their surface. The dominant signal received by NK cells is inhibitory and is provided by the interaction of its receptors with normal levels of major histocompatibility complex class I (MHC-I) molecules. If the level of MHC-I is reduced through tumorigenic or infectious processes, then this inhibitory signal is attenuated, and the NK cell is activated. As a consequence, cells with abnormal MHC-I expression become targets for lytic NK cell activity (1–3). NK cells participate in the clearance of many different viruses, and their contribution is indispensable for resisting infections by the Herpesviridae family, including cytomegalovirus (4).

Several receptor families have been identified on primate and rodent NK cells that monitor MHC-I expression on surrounding cells. These include the killer immunoglobulin-like receptors in primates and the Ly49 family in rodents (1–3). The mouse Ly49 family comprises at least 23 expressed or potential members (Ly49A–W). Although most Ly49s inhibit NK cell-mediated cytolysis after binding to MHC-I ligands, some are activating. In addition, crucial roles for Ly49 receptors in anti-

* This work was supported, in whole or in part, by National Institutes of Health Grants AI47990 (to R. A. M.) and TW007972 from the Fogarty International Center (to E. L. M.). This work was also supported by the University of Buenos Aires, the National Research Council of Argentina (CONICET), and Agencia Nacional de Promoción Científica y Técnica Grants PICT-2010-373 (to M. M. F.), PICT-2007-0632 (to J. M. D.), PICT-2010-0460 (to L. M. C.) and PICT-2008-1139 and PICT-2010-0657 (to E. L. M.).

[S] This article contains supplemental Tables S1–S3, equations, and reaction schemes.

[1] Supported by International Centre for Genetic Engineering and Biotechnology Grant CRP/ARG09-02. To whom correspondence should be addressed: Cátedra de Inmunología and IDEHU, CONICET-UBA, Facultad de Farmacia y Bioquímica, Universidad de Buenos Aires, Junín 956 4to P, 1113 Buenos Aires, Argentina. Tel.: 5411-4964-8259; Fax: 5411-4964-0024; E-mail: emalchio@ffyb.uba.ar.

[2] The abbreviations used are: NK, natural killer; MCMV, mouse cytomegalovirus; NKD, natural killer receptor domain; SPR, surface plasmon resonance; RU, response unit(s).

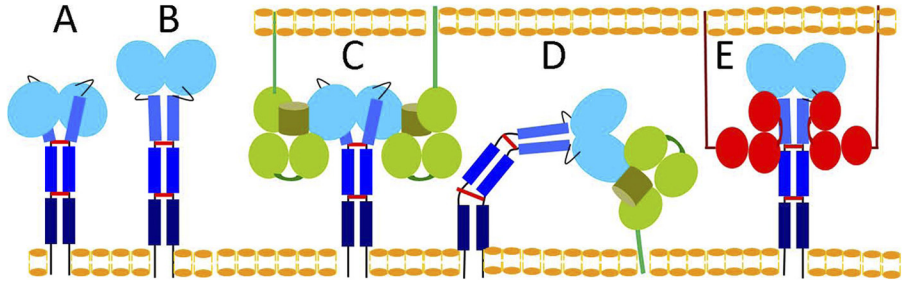

FIGURE 1. **Conformations adopted by Ly49 receptors and interaction with MHC-I and the cytomegalovirus immunoevasin m157.** *A*, the backfolded conformation of Ly49 on the NK cell membrane (*bottom*). The NKDs of the Ly49 homodimer (*blue ovals*) are backfolded onto the α-helical stalk region (*blue rectangles*) with interchain disulfides drawn as *red bars* (21). *B*, the extended conformation of Ly49 in which the NKDs extend away from the stalk. *C*, Ly49 in the backfolded conformation binding in *trans* to two MHC-I molecules (*green*) exposed on the target cell membrane (*top*) (21). The interaction with MHC-I is mediated by the NKDs. *D*, Ly49 in the extended conformation binding in *cis* to one MHC-I molecule on the same NK cell. *E*, Ly49 in the extended conformation binding *in trans* to two m157 molecules (*red*) on the target cell. The interaction with m157 is mediated by the Ly49 stalk region, not the NKDs (22).

viral immunity have been discovered. In one case, the m157 gene product of mouse cytomegalovirus (MCMV) was shown to interact directly with an inhibitory Ly49 (Ly49I) in a susceptible mouse strain (129/J) and with an activating Ly49 (Ly49H) in a resistant strain (C57BL/6) (5–7). These interactions affect the transmission of the virus and ultimately its evolutionary survival (4). In another case, the activating receptor Ly49P in MA/MyJ mice was found to confer resistance to MCMV by interacting with H-2D molecules that were modified by the MCMV protein m04 (8–11). MCMV shares many features with its human counterpart, and both viruses have developed varied and analogous immunoevasion mechanisms that involve NK cells (12). As a result, MCMV infection has become an established model to study NK cells functions, particularly the interaction of its receptors with endogenous or non-self molecules involved in viral immune control (13).

Ly49 receptors belong to the C-type lectin-like family of proteins. Ly49s are disulfide-linked homodimeric type II glycoproteins with each chain composed of a C-type lectin-like domain, which is termed the natural killer receptor domain (NKD), connected by a helical stalk of ~70 residues to the transmembrane and cytoplasmic domains (14, 15). Activating and inhibitory receptors differ with regard to their cytoplasmic domains. Considerable structural information is available for Ly49 receptors in MHC-bound and unbound forms. Crystal structures have been reported for Ly49A NKD in complex with H-2D^d (16, 17), Ly49C NKD bound to H-2K^b (18, 19), Ly49C NKD (19), Ly49I NKD (20), Ly49G2 NKD (19), Ly49L NKD (21), and Ly49L NKD with the stalk region (21). Collectively, these studies have shown that Ly49 receptors can adopt two distinct conformations: 1) a backfolded conformation in which the NKDs of the Ly49 dimer are backfolded onto the helical stalk region (Fig. 1*A*) and 2) an extended conformation in which the NKDs extend away from the stalk (Fig. 1*B*). These two conformations mediate MHC-I recognition in *trans* and *cis* (21). The backfolded conformation enables Ly49 to engage two MHC-I molecules in *trans* (Ly49 on the NK cell and MHC-I on a juxtaposed target cell) (Fig. 1*C*). By contrast, the extended conformation allows Ly49 to bind one MHC-I molecule in *cis* (Ly49 and MHC-I on the same NK cell) (Fig. 1*D*). Moreover, Ly49 receptors appear able to switch between backfolded and extended conformations (21).

Recently, the structure of Ly49H bound to the MCMV immunoevasin m157 was reported (22). This MHC-I mimic is expressed on the surface of MCMV-infected cells and adopts an MHC-I fold, although it does not bind peptides or associate with β_2-microglobulin (23). Surprisingly, m157 binds to the stalk region of Ly49H rather than the NKDs, which recognize MHC-I (Fig. 1*E*). In the complex, two m157 monomers engage the Ly49H dimer such that helical stalks lie diagonally across the α1/α2 platform of m157. This recognition mode only appears possible with Ly49 in the extended state, the conformation that recognizes MHC-I in *cis* (Fig. 1*D*). However, the binding mechanism underlying the Ly49/m157 interaction whereby a receptor that adopts two very different conformations ultimately engages two m157 ligands is unclear.

We conducted both kinetic and thermodynamic experiments to dissect the Ly49/m157 binding mechanism for the activating Ly49H and inhibitory Ly49I receptors. Combining surface plasmon resonance (SPR), fluorescence anisotropy, and circular dichroism (CD) with an exhaustive statistical analysis, we determined that the best model to describe the Ly49H/m157 and Ly49I/m157 interactions is a conformational selection mechanism involving positive cooperativity. We further established the rate-limiting step for this mechanism and characterized the reaction coordinate in terms of free energy, enthalpy, entropy, and heat capacity.

EXPERIMENTAL PROCEDURES

Protein Expression and Purification—The extracellular portion of Ly49H from mouse strain C57BL/6 (residues 88–266) comprising the NKD and most of the stalk region was cloned into the NheI and BamHI sites of the expression vector pET21a (Novagen). The protein was produced as described for Ly49L (21). Briefly, Ly49H was expressed in *Escherichia coli* BL21(DE3) as inclusion bodies; solubilized in 6 M guanidine; and folded *in vitro* by dilution into 30% (v/v) glycerol, 0.4 M arginine, 50 mM Hepes (pH 7.0), 100 mM NaCl, 3 mM reduced glutathione, and 0.8 mM oxidized glutathione. Ly49H was purified as a disulfide-linked homodimer with sequential Superdex 200 HR and Mono S columns (GE Healthcare). The extracellular portion of Ly49I from mouse strain 129/J (residues 88–269) was prepared similarly.

For the production of biotinylated Ly49H and Ly49I, an 18-residue Avi tag (MASGLNDIFEAQKIEWHE) (Avidity) was added to the N terminus of the receptors at amino acid position 88. The tagged proteins (Ly49HAvi and Ly49IAvi) were expressed in *E. coli* and purified in the same way as the wild-type proteins. Biotinylation was carried out using the enzyme BirA according to the manufacturer's protocol (Avidity).

The extracellular portion of the mature form of m157 (residues 1–285) was fused to a C-terminal His_6 tag and a protease 3C cleavage site. It was cloned into the baculovirus transfer vector pAcGP67B (BD Biosciences), which was used to produce recombinant baculovirus after co-transfection with Baculogold Bright AcMNPV DNA into the Sf9 insect cells. To produce m157, Sf9 cells cultured in Sf900 II medium (Invitrogen) were infected with the recombinant virus at a multiplicity of infection of 2 and incubated for 72 h at 27 °C. The secreted protein was purified from supernatants with Ni^{2+}nitrilotriacetic acid beads (GE Healthcare). m157 was eluted with 0.1 M Tris-HCl (pH 8.0), 0.5 M NaCl, and 0.5 M imidazole. Yields of affinity-purified m157 were typically ~10 mg/liter of culture.

Far-UV Circular Dichroism—Far-UV spectra (190–250 nm) were recorded at 25 °C using 0.1-cm quartz cuvettes with a Jasco J-810 spectropolarimeter calibrated with *d*-10-camforsulfonic acid. The scan speed was 20 nm/min with a time constant of 1 s. An average over three scans was recorded to enhance the signal to noise ratio, and buffer spectra were subtracted from all measurements.

The molar ellipticity ($[\theta]_M$ in units of degrees cm^2 $dmol^{-1}$) was calculated with the following formula (24): $[\theta]_M = 100\theta/lc$ where θ is the ellipticity in degrees obtained from the experimental spectra, l is the optical length pathway in cm, and c is equal to the molar protein concentration multiplied by the number of residues per molecule of protein.

Protein concentrations were 2 μM for Ly49H or Ly49I and 2 or 4 μM for m157 in 50 mM phosphate buffer (pH 7.4) and 150 mM NaCl. To study conformational changes in Ly49s, the receptors were incubated for 3 min at room temperature with the m157 ligand at molar ratios of Ly49 to m157 of 1:1 and 1:2 prior to data collection. These results were overlapped with the algebraic sum of the Ly49-unbound spectrum and the m157-unbound spectrum. To calculate molar ellipticity, data were normalized by the mean weight of an amino acid in each mixture. Data analysis was carried out using GraphPad Prism software and Microsoft Excel.

SPR Binding Assays—The interaction of Ly49Avi receptors with m157 was measured by SPR. All binding assays were performed at 5, 10, 15, 25, and 30 °C using a BIAcore T100 biosensor in a running buffer containing 10 mM phosphate buffer (pH 7.4) and 150 mM NaCl. Biotin-tagged Ly49HAvi or Ly49IAvi was directionally coupled to a CM5 chip onto which streptavidin had been previously immobilized via primary amine groups with an Amine Coupling kit (BIAcore). One hundred or 200 response units (RU) of each Ly49Avi receptor were immobilized on the chip. To conduct equilibrium binding and kinetic measurements, m157 was injected over two flow cells; the first was a streptavidin reference cell, and the second one was coated with Ly49HAvi or Ly49IAvi. The concentration range used for m157 was 0–12 μM. The extent of binding was calculated as the difference between the RU of the Ly49 cell and the RU of the control cell (26).

For equilibrium analyses, response levels at the maximum RU value for each concentration of ligand were plotted against m157 concentration, and the data points were fitted to the Hill equation (27). For kinetic analyses, association and dissociation data were fitted using expressions comprising summations of exponential functions (28). A Levenberg-Marquard algorithm (29) was used for the nonlinear least square fitting. A linearization method (30) was used as a first approach to interpret the interaction mechanism of the Ly49H/m157 and Ly49I/m157 couples.

Different kinetic models were assayed to interpret interaction data. All sensorgrams for the Ly49H/m157 interaction were obtained using two densities of immobilized Ly49H at different temperatures with varied flow rates and contact times. They were analyzed together and fitted globally as described by Morton *et al.* (30) and Myszka *et al.* (31) according to the differential equations for each proposed model using numerical integration with the software BIAevaluation 4.1 (BIAcore) and the Levenberg-Marquard algorithm (29). For numerical integration, a fifth-order Runge-Kutta-Fehlberg method was applied (29). We proceeded analogously with the Ly49I/m157 interaction. For thermodynamic analyses, kinetic rate constants obtained using model D (see "Results") were plotted against the inverse of temperature to construct Eyring graphs according to the classical transition state theory of absolute reaction rates (32).

Fluorescence Anisotropy Binding Assays—Ly49 receptors were labeled with fluorescein isothiocyanate (FITC) isomer I (Sigma-Aldrich). Briefly, 1 mg/ml purified Ly49H or Ly49I was dialyzed against 50 mM sodium carbonate (pH 9.5) and then incubated in a dialysis microchamber with 50 mM sodium carbonate (pH 9.5), 150 mM NaCl, and 1 mg/ml FITC for 2 days at 4 °C. The residual labeling reagents were eliminated by dialyzing the labeled protein against 10 mM phosphates (pH 7.4) and 150 mM NaCl.

Ly49-FITC (1 μM) was titrated with different concentrations of m157 (0–4 μM), and fluorescence anisotropy was measured in a Jasco FP-6500 spectrofluorometer at 25 °C when the interaction had reached equilibrium after 3-min equilibration in darkness at room temperature. The sample was excited with a polarized beam (λ_{ex} = 495 nm), and the emission was measured (λ_{em} = 520 nm) at 90° with respect to the excitation source (25).

Anisotropy was measured 15 times at each titration point, and the mean and S.D. values were calculated. A plot of anisotropy *versus* m157 concentration was constructed. An equation that links anisotropy (r) with total m157 concentration was fitted to the experimental data. Nonlinear least square data fitting was performed using Mathematica 9 software (Wolfram Research) utilizing the Levenberg-Marquard algorithm (29).

To determinate the stoichiometry of the Ly49I/m157 pair, two different titrations at different Ly49I concentrations (1 and 2.6 μM) were analyzed. The binding isotherm was deduced from these data, and a plot of the normalized signal Q, which is defined as $Q = (r - r_{min})/r_{min}$ where r is the anisotropy at each m157 concentration evaluated and r_{min} is the anisotropy of free

Ly49, *versus* the density of bound ligand indicated the stoichiometry (33–35).

RESULTS

Recombinant Protein Expression—The extracellular portions of Ly49H and Ly49I (residues 88–266 and 88–269, respectively) were recovered as disulfide-linked homodimers after *in vitro* folding from bacterial inclusion bodies as we described previously for Ly49L (21). The recombinant proteins comprise the entire NKD and most of the stalk domain, including Cys^{100}, which in the crystal structure of Ly49L (21) links two Ly49 monomers via a disulfide bond (Cys^{100}-Cys^{100}) between stalk regions. We produced soluble m157 (residues 1–285) by secretion from baculovirus-infected Sf9 insect cells.

Equilibrium SPR Analysis—As a first attempt to study the interaction between Ly49 receptors and m157, we conducted SPR experiments on the Ly49H/m157 and Ly49I/m157 pairs under equilibrium binding conditions. Ly49H and Ly49I were site-specifically biotinylated at their N termini and directionally coupled to a biosensor surface precoated with streptavidin. Different concentrations of m157 (0–12 μM) were injected over the immobilized Ly49s, and sensorgrams were recorded. This experiment was carried out at temperatures ranging between 5 and 30 °C. Fig. 2 shows plots of the maximum response in RU obtained for each m157 concentration for Ly49H and Ly49I at 25 °C. In both cases, a clear sigmoidal tendency of the experimental points was observed. Considering that the Ly49 homodimer has two possible binding sites for m157 (22), these results suggest cooperative binding.

We analyzed these plots using the Hill equation (supplemental information). Fitting of this equation to the experimental points yields an n_H coefficient of 1.7 ± 0.1 for the Ly49H/m157 pair and 1.9 ± 0.2 for the Ly49I/m157 pair. Because n_H is >1, this result is indicative of positive cooperativity for both binding pairs.

Fluorescence Anisotropy Equilibrium Analysis—To further characterize Ly49/m157 interactions, we performed fluorescence anisotropy assays under equilibrium binding conditions. Ly49s were labeled with FITC and incubated with different m157 concentrations. Fig. 3 shows fluorescence anisotropy as a function of m157 concentration. Ly49H-FITC (1 μM) and Ly49I-FITC (1 and 2.6 μM) were titrated with m157, and the fluorescence anisotropy was measured after the interaction had reached equilibrium. It was possible to establish a model that accounts for the experimental data and calculate affinity constants for each m157 binding site of the Ly49 homodimer (33, 34). Reaction schemes and equations are provided in the supplemental information.

The estimated global constants K_{G1} and K_{G2}, the sequential macroscopic constants K_{s1} and K_{s2}, and the microscopic constants k and k' for each binding site of Ly49H and Ly49I are presented in Table 1. The binding of the first m157 to the Ly49H homodimer has a K_{s1} of (5 ± 3) × 10^5 M^{-1}, and the binding of the second m157 has a K_{s2} of (3 ± 2) × 10^8 M^{-1}. The constants obtained in the case of Ly49I are similar: (5 ± 4) × 10^5 M^{-1} for binding of the first m157 and (2 ± 1) × 10^8 M^{-1} for binding of the second m157. For both receptor-ligand pairs, the second Ly49 site binds m157 with a 1000-fold higher sequential macroscopic constant than the first Ly49 site. The microscopic constants differ by 3 orders of magnitude with $k' \ggg k$. This analysis clearly indicates positive cooperativity between the two Ly49 monomers in binding m157 (33–35). The energy associated with cooperativity can be calculated as reported by Cantor and Schimmel (34). Site/site interactions stabilize the second m157 molecule strongly by ~4–5 kcal/mol over the first m157 molecule.

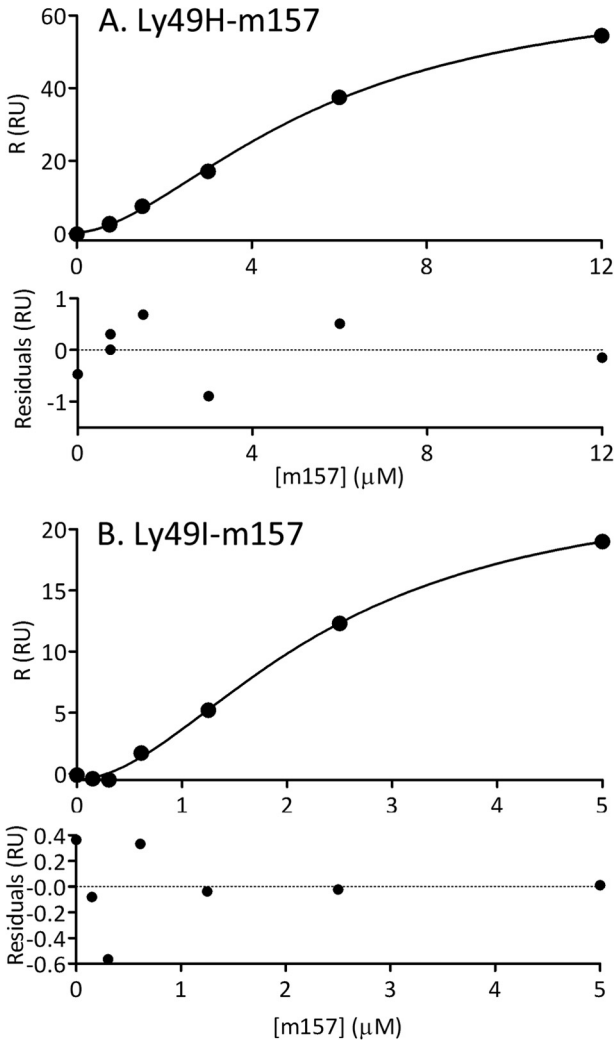

FIGURE 2. **SPR equilibrium analysis.** Plots of the maximum response (*R*) in RU obtained at each m157 total concentration assayed by injection over immobilized ~100 RU Ly49H (*A*) and Ly49I (*B*) at 25 °C. The curves describe the fitting to the Hill equation. The n_H coefficient obtained for the Ly49H/m157 pair is 1.7 ± 0.1 and for the Ly49I/m157 pair is 1.9 ± 0.2. Residual errors are indicated *below* each panel.

Determination of the Ly49I/m157 Stoichiometry—To use Reaction Scheme 1 for fluorescence anisotropy data analysis, we must know the stoichiometry of the interaction between Ly49s and m157. The stoichiometry of the Ly49H/m157 interaction was determined previously by analytical ultracentrifugation: one Ly49H dimer binds two m157 molecules (22). However, the Ly49I/m157 stoichiometry was not determined. Here, we performed an analysis of the fluorescence anisotropy data using two Ly49I-FITC concentrations, giving a plot of the normalized signal Q as a function of the bound ligand density ($\bar{\nu}$) (Fig. 4). A detailed description of this analysis is provided in the supplemental information. The maximum response Q was

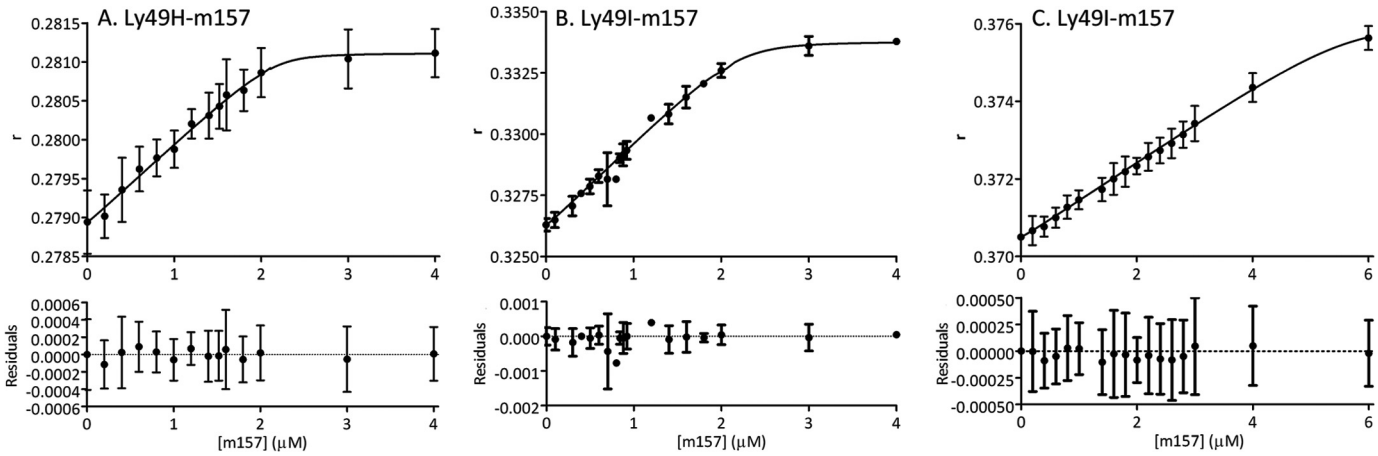

FIGURE 3. **Equilibrium fluorescence anisotropy (*r*) as a function of m157 concentration.** 1 μM Ly49H-FITC (*A*), 1 μM Ly49I-FITC (*B*), and 2.6 μM Ly49I-FITC (*C*) were titrated at 25 °C with m157, and fluorescence anisotropy was measured after the interaction had reached equilibrium. The curves describe the fitting to an equation that links the anisotropy (*r*) to the total m157 molar concentration. The constants (K_{G1}, K_{G2}, K_{s1}, K_{s2}, *k*, and *k*′) are shown in Table 1. *Error bars* represent S.D.

TABLE 1

Ly49H/m157 and Ly49I/m157 binding constants estimated with the fluorescence anisotropy assay mathematical fitting

K_{G1} and K_{G2}, global macroscopic constants; K_{s1} and K_{s2}, sequential macroscopic constants; *k* and *k*′, microscopic constants.

	$K_{G1} \times 10^5$	$K_{G2} \times 10^{13}$	$K_{s1} \times 10^5$	$K_{s2} \times 10^8$	$k \times 10^5$	$k' \times 10^8$
	M^{-1}	M^{-2}	M^{-1}	M^{-1}	M^{-1}	M^{-1}
Ly49H/m157	5 ± 3	12 ± 8	5 ± 3	3 ± 2	11 ± 6	1 ± 1
Ly49I/m157	5 ± 4	5 ± 4	5 ± 4	2 ± 1	9 ± 8	0.6 ± 0.9

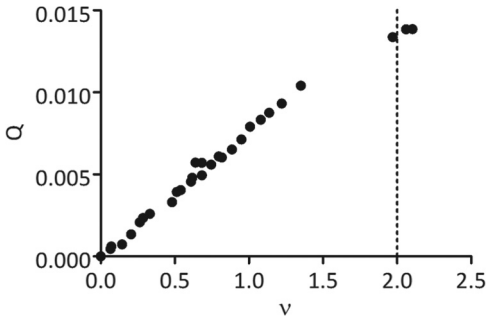

FIGURE 4. **Plot of the normalized fluorescence anisotropy signal *Q* as a function of the bound ligand density ($\bar{\nu}$).** An analysis of the fluorescence anisotropy data using two Ly49I-FITC concentrations (1 and 2.6 μM) allowed us to calculate *Q* and $\bar{\nu}$. The *dotted line* indicates that the stoichiometry of the Ly49I/m157 interaction is 1:2, the point where the response *Q* reaches its maximum value.

reached when the density of bound ligand approached 2, indicating a stoichiometry of two m157 molecules per Ly49I dimer (Fig. 4).

Far-UV CD Equilibrium Analysis Suggests Conformational Change upon Binding—A possible explanation for the increased affinity at the second site is a conformational change in Ly49 that improves the binding of the second m157 ligand. To test this hypothesis, we conducted far-UV CD experiments with Ly49 and m157. Fig. 5 shows the far-UV CD spectra of Ly49H and Ly49I alone and those obtained after incubation of Ly49 and m157 at different molar ratios compared with the algebraic sum of the Ly49 and m157 spectra. Co-incubation of both proteins produces a lower signal intensity (molar ellipticity, [θ]) than that resulting from the algebraic addition of both separate spectra, strongly suggesting that a conformational change occurs upon binding. This would lend structural support to the differences observed in the sequential macroscopic binding constants (positive cooperativity).

Kinetic SPR Analysis—After demonstrating positive cooperativity for the interaction of Ly49H and Ly49I with m157 and obtaining evidence for a conformational change upon binding, we next sought to elucidate the underlying binding mechanism by measuring the kinetics of the phenomenon and analyzing data according to Morton *et al.* (30). We performed several SPR experiments as described above at different temperatures at two different densities of Ly49 immobilized on streptavidin-coated CM5 chips using different flow rates and varying contact times. These variations were designed to rule out mass transport effects and rebinding during the dissociation phase (36) and to make the selection of a binding model more robust (26).

As a first approach to elucidate the molecular mechanism of interaction, we fitted the association and dissociation data from the sensorgrams to a sum of exponential functions (28) utilizing the Levenberg-Marquard algorithm (29). Fig. 6, *A* and *B*, show the association and dissociation SPR data, respectively, for the Ly49H/m157 and Ly49I/m157 pairs at 25 °C fitted with two-exponential functions. The residual errors are also shown and are randomly distributed. A single exponential function does not fit the experimental data well, and the χ^2 values are not further improved by using a three-exponential equation (data not shown).

In Fig. 6*C*, we plotted the first derivative of the response as a function of the response for the Ly49H/m157 and Ly49I/m157 association data. This function should give a straight line if the interaction is a simple 1:1 binding. This is not the case for any of the pairs dealt with in this study, and the plots describe a biphasic behavior.

In Fig. 6*D*, a linearization of the dissociation data is shown. Again, this function should yield a straight line if the interaction

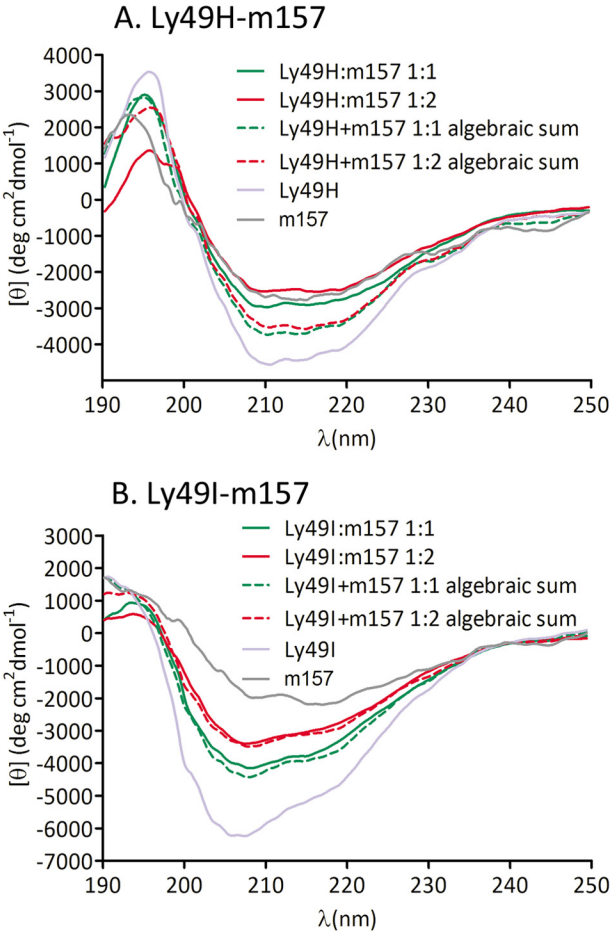

FIGURE 5. **Far-UV CD spectra of Ly49H and Ly49I in combination with m157.** Ly49H (*A*) and Ly49I (*B*) preincubated with m157 at molar ratios of 1:1 (*solid green lines*) and 1:2 (*solid red lines*) and the algebraic sum of spectra of Ly49 and one m157 molecule (*dashed green lines*) or of spectra of Ly49 and two m157 molecules (*dashed red lines*) are shown. The difference between the preincubated spectra and the algebraic sum spectra indicates a conformational change upon m157 binding. *deg*, degrees.

is a simple 1:1 binding, but instead, it renders a biphasic curve. These graphs (Fig. 6, *C* and *D*) clearly support a biphasic behavior for the interaction phenomenon in agreement with the number of exponential functions fitted in Fig. 6, *A* and *B*. This observation indicates that the binding mechanism involves at least two separate steps.

Fig. 7 shows the k_{obs} obtained after fitting a two-exponential function (Equation 11 in the supplemental information) (28) to the association data from the sensorgrams. In Fig. 7*A*, we display the k_{obs} *versus* m157 concentration corresponding to the slow exponential (k_{obs1}) function component of Equation 11 for the Ly49H/m157 and Ly49I/m157 pairs. This inverse hyperbolic dependence points to a conformational selection mechanism (37–40) where only one of the conformations of the receptor is capable of binding the ligand, and as such, this conformation is selected over the other (Reaction Scheme 1).

$$\text{Ly49} \underset{k_{-1}}{\overset{K_1}{\rightleftharpoons}} \text{Ly49*} + \text{m157} \overset{k_2}{\rightleftharpoons} \text{Ly49*/m157}$$

REACTION SCHEME 1

In Fig. 7*B*, plots of k_{obs2} *versus* m157 concentration correspond to the fast exponential function component of Equation 11 for the two interactions of the couples studied. The linear distribution of the points indicates a simple 1:1 interaction (39, 40) of the Ly49*/m157 complex with a second m157 ligand (Reaction Scheme 2).

$$\text{Ly49*/m157} + \text{m157} \underset{k_{-2}}{\overset{k_2}{\rightleftharpoons}} \text{Ly49*/(m157)}_2$$

REACTION SCHEME 2

Taking into account our results so far and the available structural information (15, 16, 18, 19, 21–23), we considered different models that could potentially describe the binding mechanism involving at least two steps (Fig. 8). For the sake of completeness, we also show in Fig. 8 the classical 1:1 Langmuir model (model A). We considered the following assumptions for generating the models that were tested to describe the interactions. 1) The stoichiometry is Ly49:m157 1:2 (one Ly49 dimer binds two m157 ligands) based on the structure of the Ly49H/m157 complex and analytical ultracentrifugation assays (22) as well as on our fluorescence anisotropy analysis of the Ly49I/m157 interaction. 2) Ly49 receptors can switch between backfolded (Ly49) and extended (Ly49*) conformations as demonstrated by x-ray crystallographic, flow cytometric, and FRET studies of Ly49 binding to MHC class I ligands (21, 41). 3) Positive cooperativity exists between the two protomers of Ly49 in agreement with the binding constants measured here by fluorescence anisotropy and the conformational change observed in our far-UV CD experiments. 4) m157 can only bind Ly49 when the latter is in the extended conformation in accordance with the structure of the Ly49H/m157 complex (22). This implies that the species Ly49/m157 (m157 bound to backfolded Ly49 protomer 1) and m157/Ly49 (m157 bound to backfolded Ly49 protomer 2) should not be considered. 5) The microspecies Ly49*/m157 (m157 bound to protomer 1) and m157/Ly49* (m157 bound to protomer 2) are equivalent. The union of the first m157 to one of the protomers is identical in nature to the union to the other protomer. This was assumed because Ly49s are symmetrical homodimers (19). 6) The conformational change between the backfolded and extended forms is concerted; that is, the two protomers are always found in the same conformation, either backfolded or extended. Mixed species of one monomer in a backfolded conformation and the other in an extended conformation do not exist. This assumption is based on crystal structures of Ly49s with stalk regions (21, 22) where the two protomers adopt the same conformation.

To decide which of the models displayed in Fig. 8 is the most appropriate for our experimental data, we applied several statistical criteria, including χ^2 (χ^2/n), modified Akaike criterion (model selection criterion), Bayesian selection criterion (Bayesian information criterion), and Hannan-Quinn information criterion to the available kinetic data. The equations of these statistics are provided in the supplemental information.

All the sensorgrams for the Ly49H/m157 couple at different temperatures with varied flow rates and contact times and different densities of immobilized Ly49 were analyzed together and fitted globally as described by Morton *et al.* (30) and

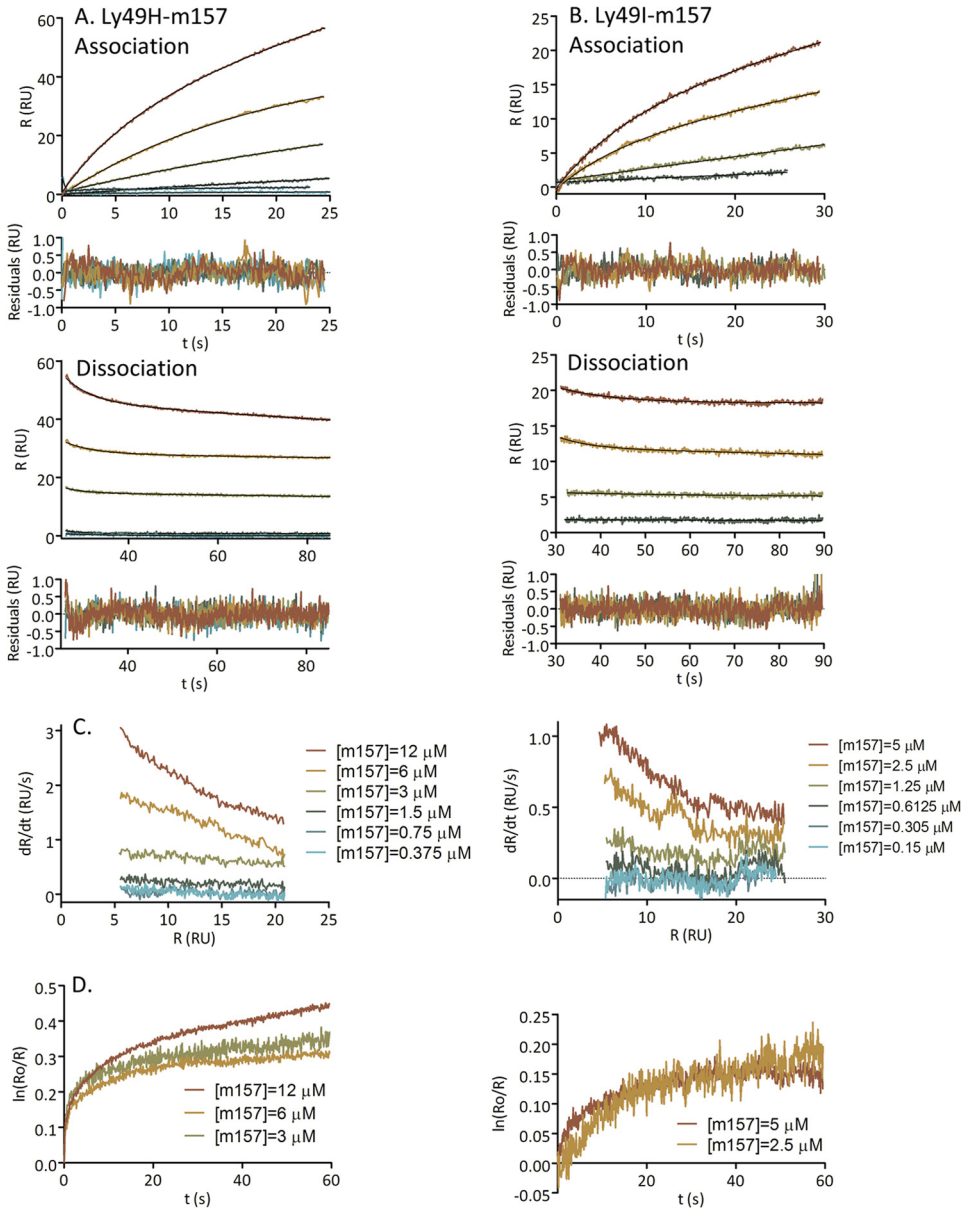

FIGURE 6. **Analysis of SPR kinetic data at 25 °C.** *A* and *B* show the association and dissociation SPR data for the Ly49H/m157 and Ly49I/m157 pairs, respectively, fitted with two-exponential functions. The residual errors appear randomly distributed and are shown *below* each panel. *C*, first derivative of the response (*R*) as a function of the response for the association data for the Ly49H/m157 (*left panel*) and Ly49I/m157 pairs (*right panel*). *D*, semilog plots of the response *versus* time for the dissociation data for the two couples analyzed. These plots (*C* and *D*) describe biphasic curves and indicate at least a two-step mechanism. This is in agreement with the fitting of two-exponential functions (*A* and *B*).

Myszka *et al.* (31) according to the differential equations derived for each proposed model by using numerical integration with the software BIAevaluation 4.1 and the Levenberg-Marquard algorithm (29). For numerical integration, a fifth-order Runge-Kutta-Fehlberg method was applied (29). We proceeded analogously with the Ly49I/m157 couple. The statistical values calculated are displayed in supplemental Tables S1 and S2 for the Ly49H/m157 and Ly49I/m157 pairs, respectively. According to these criteria, model D appears to be the best for both couples. To elucidate whether there are equally valid models to describe the interaction, we applied the Zwanzig selection criterion between two different models u and v (the equations are provided in the supplemental information). Using the latter, we compared all the models with model D.

The values obtained for the Zwanzig criterion are presented in supplemental Tables S1 and S2, and they show that models C and D appear equally plausible to describe the binding mechanism of both Ly49H/m157 and Ly49I/m157 couples. Indeed, it seems that model C explains the Ly49I/m157 interaction better than model D. Model D describes a conformational selection mechanism whereby Ly49 coexists in two different conformations (backfolded (Ly49) and extended (Ly49*)), and m157 is only capable of binding when Ly49 is in the extended conformation. The conformational change implies the slowest rate-limiting step, and the two unbound species (Ly49 and Ly49*) coexist in rapid pre-equilibrium ($k_{a2} \gg k_{d1}$). The mechanism next involves the binding of a second m157 ligand to the extended conformation of Ly49 with no further conformational

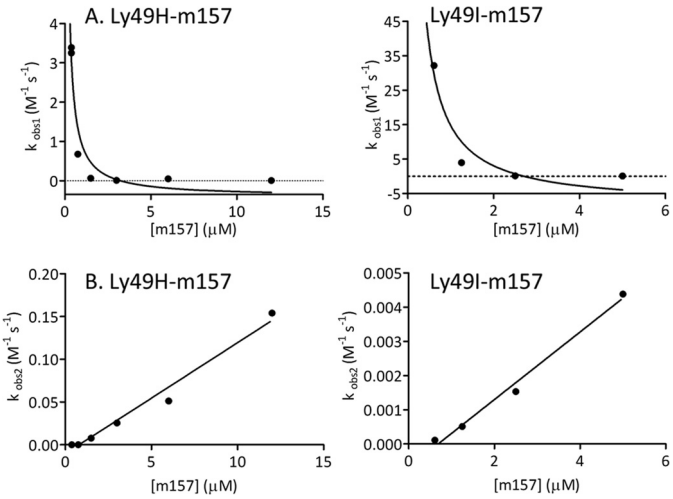

FIGURE 7. **Analysis of SPR association kinetic data at 25 °C.** k_{obs} was obtained after the fitting of a two-exponential function to the association data from the sensorgrams *versus* m157 concentration. *A*, k_{obs1} *versus* m157 concentration corresponding to the slow exponential function component for the Ly49H/m157 and Ly49I/m157 couples. These distributions correspond to a conformational selection mechanism. *B*, k_{obs2} *versus* m157 concentration corresponding to the fast exponential function component for the two interactions studied. The linear dependence of the points indicates a simple 1:1 interaction of the Ly49*/m157 complex with a second m157 ligand.

change evident. The binding of the first m157 ligand is in agreement with the behavior observed for k_{obs1} as a function of m157 concentration (Fig. 7*A*) that is typical of a conformational selection model as described earlier; and the k_{obs2} *versus* m157 concentration graph of Fig. 7*B* is also consistent with the binding of the second m157 ligand to the extended form of Ly49 with no subsequent conformational change. Model D is also compliant with the available structural data (22).

Model C describes, in the first equilibrium, a condensed step that summarizes the first two stages of model D: the conformational change between Ly49 and Ly49* and the subsequent binding of the first m157. The second equilibrium is the same as in model D. However, model C implies that the conformational change occurs *only as a consequence* of the first binding event (*i.e.* it ignores the pre-existence of forms Ly49 and Ly49* prior to binding). In addition, model D is in agreement with Figs. 6 and 7. Consequently, we consider that model D is the most appropriate to describe both the Ly49H/m157 and Ly49I/m157 binding mechanisms.

Fig. 9 shows the sensorgrams for the Ly49H/m157 and Ly49I/m157 pairs at temperatures of 5, 10, 15, 25, and 30 °C with the fitted curves using model D. The kinetic rate constants (association rate k_a and dissociation rate k_d) and macroscopic sequential equilibrium constants (K_{A1} for the conformational change equilibrium, K_{A2} for the binding of the first m157, and K_{A3} for the binding of the second m157) determined with SPR data analyzed using numerical integration of the differential equations of model D are shown in Tables 2 and 3 for both complexes Ly49H/m157 and Ly49I/m157.

It is important to note that the macroscopic sequential constants K_{A2} and K_{A3} calculated ($K_A = k_a/k_d$) from kinetic analysis of SPR data are consistent with the constants K_{s1} and K_{s2} determined by the fluorescence anisotropy assays. Both K_{A2} and K_{s1} are $\sim 10^5\ \text{M}^{-1}$, and K_{A3} and K_{s2} are $\sim 10^8\ \text{M}^{-1}$. This validates results obtained by different methods, integrating both kinetic and thermodynamic experiments into a consistent picture.

Thermodynamic Analysis of Ly49/m157 Interactions—To complete our study of Ly49 binding to m157, we performed an Eyring analysis using the kinetic rate constants obtained from applying model D to the SPR data (42). The dependence of these constants on temperature is plotted in Fig. 10 for the Ly49H/m157 and Ly49I/m157 pairs. The Eyring equation was fitted to the experimental points at the reference temperature of 25 °C to render the thermodynamic activation parameters $\Delta H_o^{\ddagger}$ (activation enthalpy), $\Delta S_o^{\ddagger}$ (activation entropy), and $\Delta Cp_o^{\ddagger}$ (activation heat capacity) (supplemental Table S3). The $\Delta G_o^{\ddagger}$ (activation free energy) was also calculated from the kinetic rate constants.

A landscape depicting the progression of the reaction at 25 °C is shown in Fig. 11 for the free energy (Fig. 11*A*) together with its deconvolution into enthalpic (Fig. 11*B*) and entropic (Fig. 11*C*) components for Ly49H/m157 and Ly49I/m157 interactions. This figure shows that the rate-limiting step in the process can be attributed to the conformational change from the backfolded to the extended form. An enthalpic barrier of ~30 kcal/mol limits the process, which becomes spontaneous due to an entropy increase. By contrast, the subsequent binding of two m157 ligands to the extended form of Ly49 is characterized by small entropic barriers to form the transition state that are compensated by a favorable enthalpic release of energy. Overall, the global thermodynamic parameters from the initial state (free forms of backfolded Ly49 and m157) to the final state (Ly49*/$(m157)_2$ complex) are characterized by an enthalpy increase in the system (endothermic reaction) that is compensated by an entropy increase, making the interaction spontaneous.

DISCUSSION

In this work, we exhaustively characterized the interaction of Ly49H and Ly49I with the immunoevasin m157 from MCMV. We determined the constants that govern m157 binding to the first and the second protomer of Ly49 and demonstrated that ligand engagement involves positive cooperativity. We arrived at this conclusion by performing complementary kinetic and thermodynamic experiments. Finally, we determined the model that best describes the binding mechanism and conducted a thermodynamic analysis to define the energy landscape of the Ly49/m157 interaction.

The sequential macroscopic constants K_{s1} and K_{s2} measured by fluorescence anisotropy and the equilibrium constants K_{A2} and K_{A3} derived from SPR data differ from values reported in previous studies (22, 23). K_{s1} and K_{A2} correspond to the binding of the first m157 ligand to the Ly49 protomer and are in the $\sim 10^5\ \text{M}^{-1}$ range. On the other hand, K_{s2} and K_{A3} correspond to the binding of the second m157 ligand to the other Ly49 protomer and fall in the $\sim 10^8\ \text{M}^{-1}$ range. The binding constants determined by Adams *et al.* (23) using SPR were $K_D = 166$ nM ($K_A = 6 \times 10^6\ \text{M}^{-1}$) for Ly49I/m157 interaction and $K_D = 1\ \mu$M ($K_A = 1 \times 10^6\ \text{M}^{-1}$) for Ly49H/m157 interaction. The K_D measured by Berry *et al.* (22) for the Ly49H/m157 couple using SPR was $K_D = 81.0\ \mu$M ($K_A = 1.23 \times 10^4\ \text{M}^{-1}$). The differences can be explained by the following factors. 1) m157 used by Berry *et*

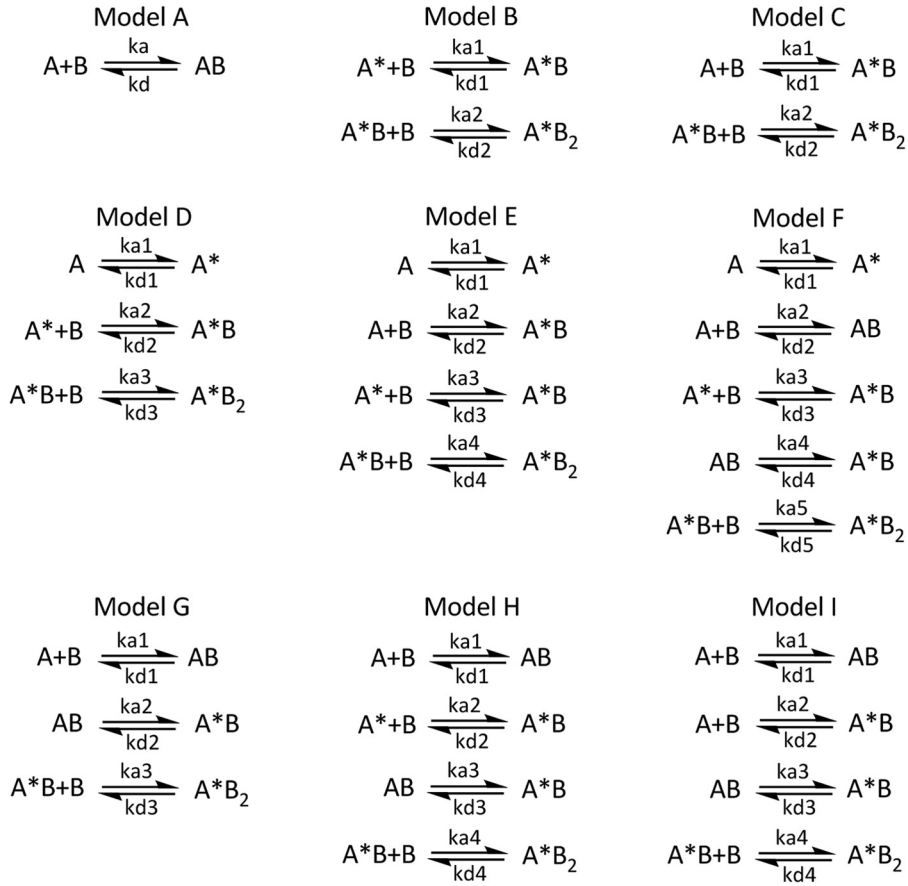

FIGURE 8. **Proposed models for the binding mechanism between Ly49 and m157.** Models of the Ly49H/m157 and Ly49I/m157 interactions should include at least two steps according to the assumptions described in the text. *A*, backfolded Ly49; *A**, extended Ly49; *B*, m157.

al. (22) is derived from the G1F strain of MCMV instead of the Smith strain for the m157 used by Adams *et al.* (23) and in this study. These m157 molecules differ in several amino acids located at the interface with Ly49 (22). 2) The amounts of Ly49 immobilized on biosensor surfaces in the previous studies (~500 RU by Berry *et al.* (22) and ~600 RU by Adams *et al.* (23)) are 5–6 times higher than the amounts immobilized in our study (~100 RU). High surface densities amplify mass transport effects, thereby altering the binding kinetics and blurring the interaction mechanism (26). 3) In both previous studies, the sensorgrams and plots derived from the SPR experiments were only analyzed using a Langmuir 1:1 interaction model. By contrast, we performed statistic calculations to decide which of the hypothesized models gave the best fit and used this model to estimate binding constants from the SPR data. We also determined the binding constants using fluorescence anisotropy, an independent solution technique useful for the purpose of validating SPR data. Had we fitted our sensorgrams to a simple Langmuir 1:1 model, the resulting K_A value would have been $\sim 10^6$ M^{-1}. This value agrees with the K_A value reported by Adams *et al.* (23) but not with that of Berry *et al.* (22) possibly because of the different MCMV strain sources of m157 as noted above. This exercise highlights the importance of a judicious choice of the binding model as a prerequisite for a correct interpretation of quantitative results.

In accordance with previous evidence derived from flow cytometric and FRET studies of Ly49A (21, 41), we detected different Ly49 conformations by using a CD assay. Back *et al.* (21) showed that the two states of Ly49A, backfolded and extended, co-exist and mediate *trans* and *cis* interactions, respectively, with MHC class I. In our far-UV CD experiments, the spectra indicate that a conformational change occurs when m157 binds to Ly49. The changes in spectral intensities may represent a conformational equilibrium displacement from the backfolded form, which is the predominant (or default) conformation of Ly49s in the absence of ligand (21), to the extended form, which is available to bind m157 (22).

We first attempted to understand the binding mechanism by fitting exponential functions to kinetic data using the linearization method described by Morton *et al.* (30) as a litmus test. This approach indicates that there are at least two successive hemireactions and led us to propose several different mechanisms that could explain the SPR data. After applying numerous statistical methods, we concluded that a conformational selection model (model D in Fig. 8) is the most appropriate for describing the Ly49/m157 interaction. This model includes the least number of assumptions necessary to explain the experimental data (Occam's razor criterion): the first rate-limiting step of conformational change from the backfolded to the extended form of Ly49 present in rapid pre-equilibrium ($k_{a2} \gg k_{d1}$) and two successive steps corresponding to the binding of the first and second m157 ligands. Significant interaction energy is associated with this two-step binding phenomenon (~4–5 kcal/mol).

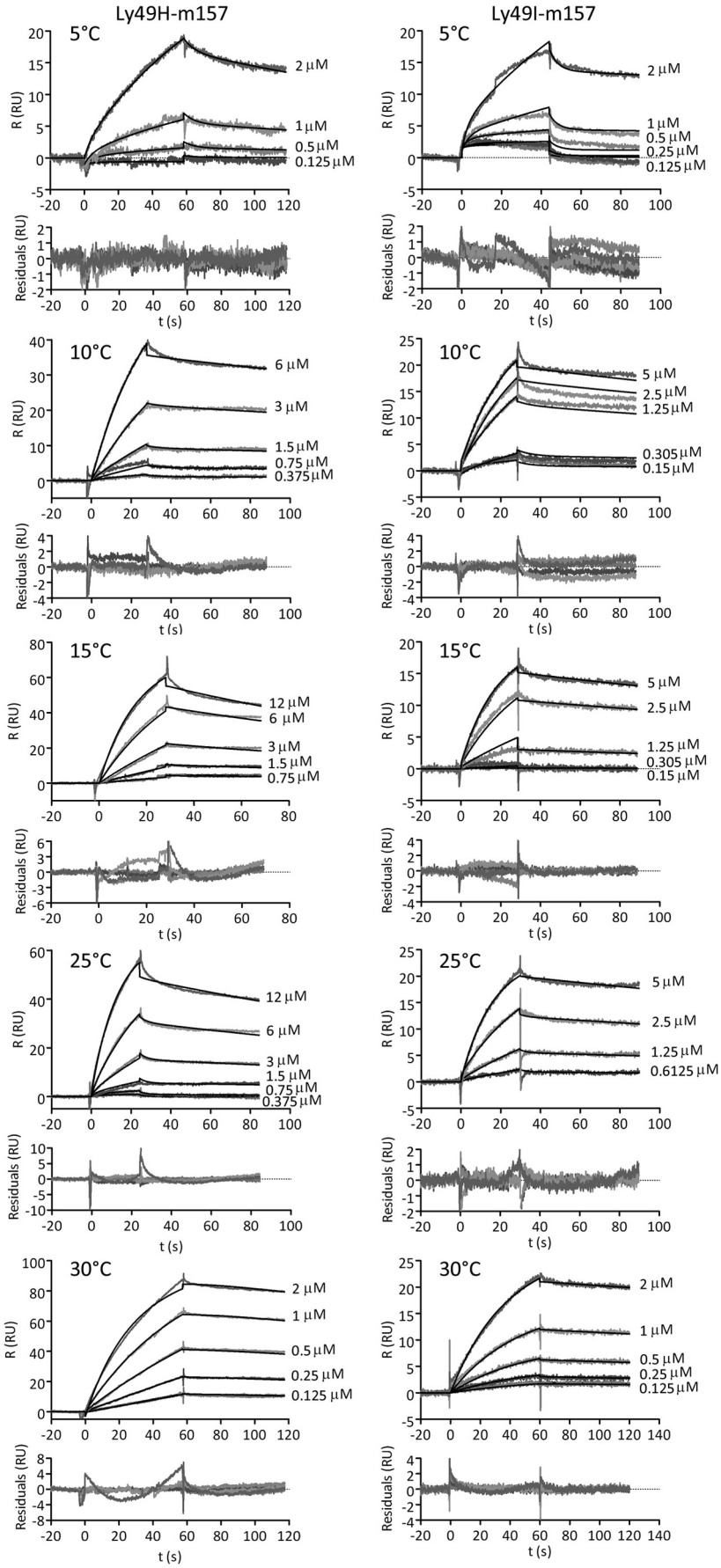

TABLE 2
Ly49H/m157 and Ly49I/m157 kinetic rate constants estimated from the SPR kinetic analysis with model D at different temperatures

T	$k_{a1} \times 10^{-5}$	$k_{d1} \times 10^{-3}$	$k_{a2} \times 10^{3}$	k_{d2}	$k_{a3} \times 10^{5}$	$k_{d3} \times 10^{-3}$
℃	s^{-1}	s^{-1}	$M^{-1}\,s^{-1}$	s^{-1}	$M^{-1}\,s^{-1}$	s^{-1}
Ly49H/m157						
5	510 ± 20	0.02 ± 0.01	2.8 ± 0.1	0.130 ± 0.003	0.52 ± 0.01	3.69 ± 0.09
10	0.02 ± 0.01	13 ± 1	10.7 ± 0.2	0.97 ± 0.08	6.8 ± 0.5	2.56 ± 0.04
15	0.653 ± 0.008	12 ± 5	58 ± 3	0.99 ± 0.07	52 ± 3	107 ± 11
25	0.4 ± 0.1	18 ± 1	6.99 ± 0.08	1.58 ± 0.02	16.1 ± 0.2	5.63 ± 0.05
30	0.3 ± 0.1	10.2 ± 0.7	24.5 ± 0.3	0.0159 ± 0.0009	30.5 ± 0.9	8.9 ± 0.8
Ly49I/m157						
5	59 ± 5	0.6 ± 0.3	12.4 ± 0.5	0.176 ± 0.004	0.312 ± 0.007	0.12 ± 0.01
10	20 ± 10	12 ± 3	26.2 ± 0.2	0.43 ± 0.03	43 ± 3	2.60 ± 0.07
15	0.9 ± 0.3	10.4 ± 0.5	68 ± 3	4.14 ± 0.06	4.4 ± 0.2	3.05 ± 0.06
25	180 ± 60	0.0266 ± 0.0004	16.8 ± 0.1	0.396 ± 0.002	2.65 ± 0.02	2.01 ± 0.02
30	740 ± 10	0.0100 ± 0.0007	4.28 ± 0.07	0.00093 ± 0.00006	0.04 ± 0.02	0.04 ± 0.02

TABLE 3
Ly49H/m157 and Ly49I/m157 binding equilibrium constants estimated from the SPR kinetic analysis with model D at different temperatures calculated as $K_A = k_a/k_d$

T	K_{A1}	$K_{A2} \times 10^{4}$	$K_{A3} \times 10^{8}$
℃		M^{-1}	M^{-1}
Ly49H/m157			
5	330 ± 40	2.2 ± 0.1	0.140 ± 0.001
10	(1 ± 1) × 10^{-5}	1.1 ± 0.1	2.7 ± 0.2
15	(6 ± 2) × 10^{-4}	5.9 ± 0.7	0.49 ± 0.08
25	(2.4 ± 0.9) × 10^{-4}	0.44 ± 0.01	2.86 ± 0.06
30	(3 ± 2) × 10^{-4}	15 ± 1	3.4 ± 0.4
Ly49I/m157			
5	1.0 ± 0.6	7.0 ± 0.4	2.5 ± 0.3
10	0.02 ± 0.01	6.1 ± 0.5	17 ± 2
15	(8 ± 3) × 10^{-4}	1.6 ± 0.1	1.4 ± 0.1
25	70 ± 20	4.25 ± 0.05	1.32 ± 0.02
30	740 ± 60	460 ± 30	1 ± 1

To investigate whether this conformational selection mechanism might also apply to Ly49 binding to MHC-I, we conducted SPR assays for the Ly49P/H-2D^{k}, Ly49H/H-2D^{d}, and Ly49I/H-2D^{d} interaction pairs.[3] However, we did not observe a sigmoidal tendency in plots of maximum response *versus* ligand concentration as is the case for both Ly49H/m157 and Ly49I/m157 interactions. This finding is readily explained by the ability of MHC-I to engage Ly49 in both the backfolded (in *trans*) and extended (in *cis*) conformations (21), whereas m157 can only bind Ly49 in the extended conformation (22). Because unbound Ly49 exists predominantly in the backfolded state (21), no shift to the extended state would be necessary for MHC-I to bind.

When the encounter of two molecules is the rate-limiting step, the reaction is diffusion-controlled, and when formation of the transition state is rate-limiting, the reaction is controlled by the height of the activation energy barrier (43). The k_{a2} and k_{a3} values for the interactions studied here ($k_{a2} \sim 10^{3}\ M^{-1}\ s^{-1}$ and $k_{a3} \sim 10^{5}\ M^{-1}\ s^{-1}$) are 3–6 orders of magnitude lower than typical k_a maximum values for diffusion-controlled mechanisms involving the collision of two uncharged and uniformly reactive spheres ($\sim 3 \times 10^{9}\ M^{-1}\ s^{-1}$) as defined by De La Cruz and Pollard (44). In addition, the $\Delta H_o^{\ddagger}$ values we obtained for Ly49/m157 association reactions (around −10 to −20 kcal/mol) are higher than the reported values for diffusion-limited reactions in water (around −4 to −5 kcal/mol) (45). Therefore, we conclude that Ly49/m157 binding is activation energy-controlled with the formation of a transition state that implies a substantial energy barrier. In addition, the constants k_{a1} and k_{d1} corresponding to the conformational change equilibrium are

[3] P. N. Romasanta, L. M. Curto, N. Urtasun, M. B. Sarratea, S. Chiappini, M. V. Miranda, J. M. Delfino, R. A. Mariuzza, M. M. Fernández, and E. L. Malchiodi, unpublished results.

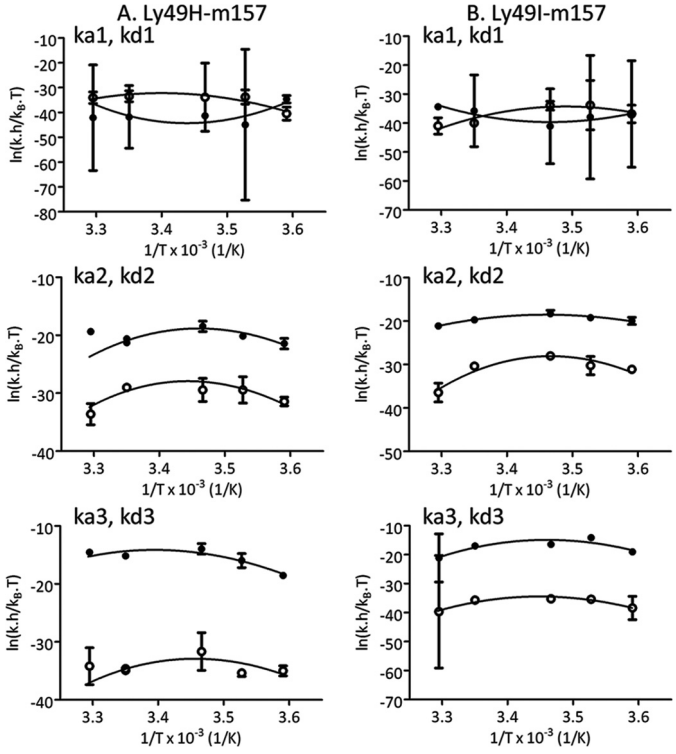

FIGURE 10. **Eyring analysis using kinetic rate constants at different temperatures.** Eyring analysis using the kinetic rate constants obtained after applying model D to the SPR data for the Ly49H/m157 (*A*) and Ly49I/m157 interactions (*B*) is shown. The Eyring equation was fitted to experimental data points at 25 °C to obtain the thermodynamic activation parameters $\Delta H_o^{\ddagger}$, $\Delta S_o^{\ddagger}$, and $\Delta Cp_o^{\ddagger}$ (supplemental Table S3). *Filled circles* indicate association data, and *empty circles* indicate dissociation data. *Error bars* represent S.D.

FIGURE 9. **Sensorgrams for Ly49/m157 interactions at different temperatures.** Sensorgrams for the Ly49H/m157 and for Ly49I/m157 interactions at 5, 10, 15, 25, and 30 °C are shown. On the side of each sensorgram, the total m157 molar concentration assayed is indicated. *Black lines* indicate the fitted curves using numerical integration with BIAevaluation 4.1 software from the differential equations of model D. The kinetic rate constants and macroscopic sequential equilibrium constants are shown in Tables 2 and 3, respectively, for the Ly49H/m157 and Ly49I/m157 pairs. *R*, response.

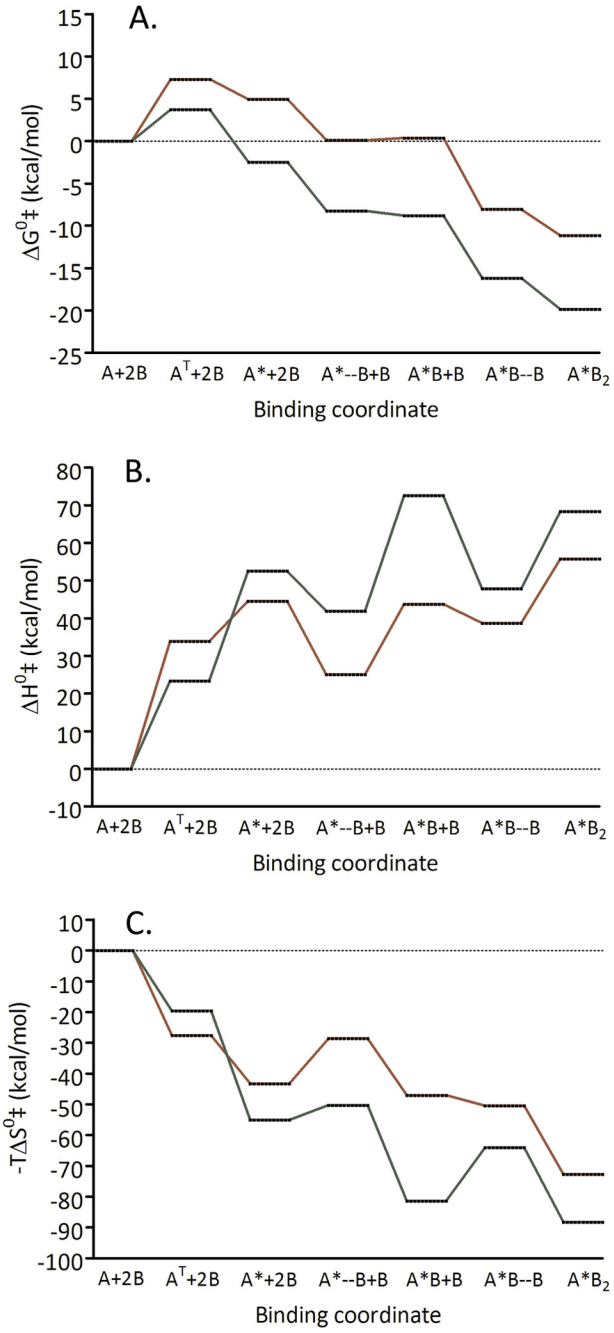

FIGURE 11. **Reaction progress landscapes at 25 °C.** Reaction progress landscapes at 25 °C for the free energy (*A*) together with the deconvolution into enthalpic (*B*) and entropic (*C*) components for the Ly49H/m157 (*red*) and Ly49I/m157 pairs (*green*) are shown. This figure shows that the global rate-limiting step is a conformational change from the backfolded to the extended state of Ly49. *A*, backfoldedLy49; *A**, extended Ly49; *B*, m157; A^T, Ly49 in transition state for the conformational change step; *A*–B*, transition state for the binding to the first m157; *A*B*, extended Ly49 bound to one m157 molecule; *A*B–B*, transition state for the binding to the second m157; A^*B_2, extended Ly49 bound to two m157 molecules.

$\sim 10^{-5}$ and 10^{-3} s^{-1}, respectively. This indicates that the equilibrium is displaced to the backfolded Ly49 form when there is no ligand ($K_{A1} \sim 10^{-2}$), an observation in agreement with crystallographic studies of Ly49 (21).

In examining the rate constants that describe the binding of the first and second m157 to the extended states of Ly49H and Ly49I, we found the relationships $k_{a3} > k_{a2}$ and $k_{d3} < k_{d2}$, which make $K_{A3} > K_{A2}$. Thus, the Ly49*/$(m157)_2$ complex forms faster and dissociates more slowly than the Ly49*/m157 complex. This difference can be explained by assuming that the step describing the interaction of the first m157 is influenced and conditioned by the first conformational equilibrium, effectively slowing down the binding of the first ligand. The global rate-limiting energy barrier must be overcome when the first m157 is added (Fig. 11*A*). The high dissociation rate k_{d2} could be due to the presence of very unstable species of the type Ly49/m157 (m157 bound to the backfolded state), which dissociates rapidly. In addition, the Ly49*/m157 species has a stability very similar to the transition state (Fig. 11*A*), making dissociation a more frequent event. The observed increase in the association rate for the second m157 may be explained by the availability of the second site once Ly49 adopts the extended conformation. The dissociation rate k_{d3} is slower than kd_2 due to the high stability of the final complex Ly49*/$(m157)_2$ (ΔG^0 between −10 and −20 kcal/mol).

The free activation energy landscapes in Fig. 11*A* may be deconvoluted into enthalpic (Fig. 11*B*) and entropic (Fig. 11*C*) components. An enthalpic barrier (positive $\Delta H_o^{\ddagger}$) of ~40–50 kcal/mol must be overcome to achieve the extended form of Ly49 (Fig. 11*B*), indicating that the conformational transition requires energy to break hydrogen bonds and other contacts between water molecules and amino acid residues and among residues themselves. Indeed, in the crystal structure of backfolded Ly49, the stalk region makes numerous contacts with the NKDs that would be lost upon extension (21). However, this step has a favorable entropy (positive $T\Delta S_o^{\ddagger}$) (Fig. 11*C*), which acts as a driving force for the reaction, implying greater flexibility of the extended compared with the backfolded conformations. The $\Delta Cp_o^{\ddagger}$ value for the transition from the backfolded to the extended form is positive (~2 kcal/mol), suggesting solvent exposure of hydrophobic surfaces (46–48), a picture consistent with the available structural data (21). By contrast, the binding of the first and second m157 ligands to the extended form of Ly49 is characterized by a favorable enthalpy (negative $\Delta H_o^{\ddagger}$), unfavorable entropy (negative $T\Delta S_o^{\ddagger}$) (Fig. 11, *B* and *C*), and negative $\Delta Cp_o^{\ddagger}$, indicating formation of productive contacts between Ly49 and m157, decreased flexibility, and burial of hydrophobic surface at the complex interface.

We have shown that Ly49 NK receptors bind m157 by a mechanism involving positive cooperativity and conformational selection and that this mechanism correlates well with the available crystal structures. In addition, we have shown that inhibitory and activating Ly49s use the same mechanism to bind m157. Therefore, differences in signaling are due entirely to differences in the cytoplasmic domains of Ly49s whereby inhibitory Ly49s transduce signals via immunoreceptor tyrosine-based inhibitory motifs, whereas activating Ly49s instead use the signaling homodimer DAP12.

Acknowledgments—We are grateful to S. K. Anderson (National Cancer Institute) and A. P. Makrigiannis (Clinical Research Institute of Montreal) for Ly49 cDNAs.

REFERENCES

1. McQueen, K. L., and Parham, P. (2002) Variable receptors controlling activation and inhibition of NK cells. *Curr. Opin. Immunol.* **14,** 615–621

2. Yokoyama, W. M., and Plougastel, B. F. (2003) Immune functions encoded by the natural killer gene complex. *Nat. Rev. Immunol.* **3,** 304–316
3. Lanier, L. L. (2005) NK cell recognition. *Annu. Rev. Immunol.* **23,** 225–274
4. Lanier, L. L. (2008) Evolutionary struggles between NK cells and viruses. *Nat. Rev. Immunol.* **8,** 259–268
5. Arase, H., Mocarski, E. S., Campbell, A. E., Hill, A. B., and Lanier, L. L. (2002) Direct recognition of cytomegalovirus by activating and inhibitory NK cell receptors. *Science* **296,** 1323–1326
6. Smith, H. R., Heusel, J. W., Mehta, I. K., Kim, S., Dorner, B. G., Naidenko, O. V., Iizuka, K., Furukawa, H., Beckman, D. L., Pingel, J. T., Scalzo, A. A., Fremont, D. H., and Yokoyama, W. M. (2002) Recognition of a virus-encoded ligand by a natural killer cell activation receptor. *Proc. Natl. Acad. Sci. U.S.A.* **99,** 8826–8831
7. Corbett, A. J., Coudert, J. D., Forbes, C. A., and Scalzo, A. A. (2011) Functional consequences of natural sequence variation of murine cytomegalovirus m157 for Ly49 receptor specificity and NK cell activation. *J. Immunol.* **186,** 1713–1722
8. Desrosiers, M. P., Kielczewska, A., Loredo-Osti, J. C., Adam, S.G., Makrigiannis, A. P., Lemieux, S., Pham, T., Lodoen, M. B., Morgan, K., Lanier, L. L., and Vidal, S. M. (2005) Epistasis between mouse Klra and major histocompatibility complex class I loci is associated with a new mechanism of natural killer cell-mediated innate resistance to cytomegalovirus infection. *Nat. Genet.* **37,** 593–599
9. Dighe, A., Rodriguez, M., Sabastian, P., Xie, X., McVoy, M., and Brown, M. G. (2005) Requisite H2k role in NK cell-mediated resistance in acute murine cytomegalovirus-infected MA/My mice. *J. Immunol.* **175,** 6820–6828
10. Xie, X., Dighe, A., Clark, P., Sabastian, P., Buss, S., and Brown, M. G. (2007) Deficient major histocompatibility complex-linked innate murine cytomegalovirus immunity in MA/My.L-H2 mice and viral downregulation of H-2 class I proteins. *J. Virol.* **81,** 229–236
11. Kielczewska, A., Pyzik, M., Sun, T., Krmpotic, A., Lodoen, M. B., Munks, M. W., Babic, M., Hill, A. B., Koszinowski, U. H., Jonjic, S., Lanier, L. L., and Vidal, S. M. (2009) Ly49P recognition of cytomegalovirus-infected cells expressing H2-D and CMV-encoded m04 correlates with the NK cell antiviral response. *J. Exp. Med.* **206,** 515–523
12. Lisnić, V. J., Krmpotić, A., and Jonjić, S. (2010) Modulation of natural killer cell activity by viruses. *Curr. Opin. Microbiol.* **13,** 530–539
13. Pyzik, M., Gendron-Pontbriand, E. M., and Vidal, S. M. (2011) The impact of Ly49-NK cell-dependent recognition of MCMV infection on innate and adaptive immune responses. *J. Biomed. Biotechnol.* **2011,** 641702
14. Natarajan, K., Dimasi, N., Wang, J., Mariuzza, R. A., and Margulies, D. H. (2002) Structure and function of natural killer cell receptors: multiple solutions to self, nonself discrimination. *Annu. Rev. Immunol.* **20,** 853–885
15. Deng, L., and Mariuzza, R. A. (2006) Structural basis for recognition of MHC and MHC-like ligands by natural killer cell receptors. *Semin. Immunol.* **18,** 159–166
16. Tormo, J., Natarajan, K., Margulies, D. H., Mariuzza, R. A. (1999) Crystal structure of a lectin-like natural killer cell receptor bound to its MHC class I ligand. *Nature* **402,** 623–631
17. Dam, J., Baber, J., Grishaev, A., Malchiodi, E. L., Schuck, P., Bax, A., and Mariuzza, R. A. (2006) Variable dimerization of the Ly49A natural killer cell receptor results in differential engagement of its MHC class I ligand. *J. Mol. Biol.* **362,** 102–113
18. Dam, J., Guan, R., Natarajan, K., Dimasi, N., Chlewicki, L. K., Kranz, D. M., Schuck, P., Margulies, D. H., and Mariuzza, R. A. (2003) Variable MHC class I engagement by Ly49 natural killer cell receptors demonstrated by the cristal structure of Ly49C bound to H-2K^b. *Nat. Immunol.* **4,** 1213–1222
19. Deng, L., Cho, S., Malchiodi, E. L., Kerzic, M. C., Dam, J., and Mariuzza, R. A. (2008) Molecular architecture of the MHC-binding site of Ly49 natural killer cell receptors. *J. Biol. Chem.* **283,** 16840–16849
20. Dimasi, N., Sawicki, M. W., Reineck, L. A., Li, Y., Natarajan, K., Margulies, D. H., and Mariuzza, R. A. (2002) Crystal structure of the Ly49I natural killer cell receptor reveals variability in dimerization mode within the Ly49 family. *J. Mol. Biol.* **320,** 573–585
21. Back, J., Malchiodi, E. L., Cho, S., Scarpellino, L., Schneider, P., Kerzic, M.C., Mariuzza, R. A., and Held, W. (2009) Distinct conformations of Ly49 natural killer cell receptors mediate MHC class I recognition in *trans* and *cis*. *Immunity* **31,** 598–608
22. Berry, R., Ng, N., Saunders, P. M., Vivian, J. P., Lin, J., Deuss, F. A., Corbett, A. J., Forbes, C. A., Widjaja, J. M., Sullivan, L. C., McAlister, A. D., Perugini, M. A., Call, M. J., Scalzo, A. A., Degli-Esposti, M. A., Coudert, J. D., Beddoe, T., Brooks, A. G., and Rossjohn, J. (2013) Targeting of a natural killer cell receptor family by a viral immunoevasin. *Nat. Immunol.* **14,** 699–705
23. Adams, E. J., Juo, Z. S., Venook, R. T., Boulanger, M. J., Arase, H., Lanier, L. L., and Garcia, K. C. (2007) Structural elucidation of the m157 mouse cytomegalovirus ligand for Ly49 natural killer cell receptors. *Proc. Natl. Acad. Sci. U.S.A.* **104,** 10128–10133
24. Schmid, F. X. (1989) in *Protein Structure: a Practical Approach* (Creighton T. E., ed), pp. 251–285, IRL Press, New York
25. Lakowicz, J. R. (2006) *Principles of Fluorescence Spectroscopy*, 3rd Ed., pp. 353–382, Springer, New York
26. Myszka, D. G. (1997) Kinetic analysis of macromolecular interactions using surface plasmon resonance biosensors. *Curr. Opin. Biotechnol.* **8,** 50–57
27. Hill, A. V. (1910) The possible effects of the aggregation of the molecules of hemoglobin on its dissociation curves. *J. Physiol.* **40,** 4–7
28. O'Shannessy, D. J., Brigham-Burke, M., Soneson, K. K., Hensley, P., and Brooks, I. (1993) Determination of rate and equilibrium binding constants for macromolecular interactions using surface plasmon resonance, use of nonlinear least squares analysis methods. *Anal. Biochem.* **212,** 457–468
29. Press, W. H., Teukolsky, S. A., Vetterling, W. T., and Flannery, B. P. (1999) *Numerical Recipes in C*, 2nd Ed., pp. 801–806, Cambridge University Press, Cambridge, UK
30. Morton, T. A., Myszka, D. G., and Chaiken, I. M. (1995) Interpreting complex binding kinetics from optical biosensors: a comparison of analysis by linearization, the integrated rate equation, and numerical integration. *Anal. Biochem.* **227,** 176–185
31. Myszka, D. G., Morton, T. A., Doyle, M. L., and Chaiken, I. M. (1997) Kinetic analysis of a protein antigen-antibody interaction limited by mass transport on an optical biosensor. *Biophys. Chem.* **64,** 127–137
32. Gutfreund, H. (1995) *Kinetics for the Life Sciences: Receptors, Transmitters and Catalysts*, pp. 236–247, Cambridge University Press, Cambridge, UK
33. Hill, T. L. (1985) *Cooperativity Theory in Biochemistry: Steady-state and Equilibrium Systems*, pp. 59–87, Springer-Verlag, New York
34. Cantor, C. R., and Schimmel, P. R. (1980) *Biophysical Chemistry: Parts I–III*, pp. 849–886, W. H. Freeman, San Francisco
35. Weber, G. (1992) Protein Interactions, pp. 1–287, Chapman and Hall, New York
36. O'Shannessy, D. J., and Winzor, D. J. (1996) Interpretation of deviations from pseudo-first-order kinetic behavior in the characterization of ligand binding by biosensor technology. *Anal. Biochem.* **236,** 275–283
37. Monod, J., Wyman, J., and Changeux, J. P. (1965) On the nature of allosteric transitions: a plausible model. *J. Mol. Biol.* **12,** 88–118
38. Tsai, C. J., Ma, B., Sham, Y. Y., Kumar, S., and Nussinov, R. (2001) Structured disorder and conformational selection. *Proteins* **44,** 418–427
39. Zhou, H. X. (2010) Rate theories for biologists. *Q. Rev. Biophys.* **43,** 219–293
40. Creighton, T. E. (2010) *The Physical and Chemical Basis of Molecular Biology*, pp. 91–114, Helvetian Press, East Sussex, UK
41. Back, J., Angelov, G. S., Mariuzza, R. A., and Held, W. (2011) The interaction with H-2D^d in *cis* is associated with a conformational change in the Ly49A NK cell receptor. *Front. Immunol.* **2,** 55
42. Winzor, D. J., and Jackson, C. M. (2006) Interpretation of the temperature dependence of equilibrium and rate constants. *J. Mol. Recognit.* **19,** 389–407
43. Chen, J., Makabe, K., Nakamura, T., Inobe, T., and Kuwajima, K. (2011) Dissecting a bimolecular process of $MgATP^{2-}$ binding to chaperonin GroEL. *J. Mol. Biol.* **410,** 343–356
44. De La Cruz, E. M., and Pollard, T. D. (1995) Nucleotide-free actin: stabilization by sucrose and nucleotide binding kinetics. *Biochemistry* **34,** 5452–5461

45. Lohman, T. M. (1986) Kinetics of protein-nucleic acid interactions—use of salt effects to probe mechanisms of interaction. *CRC Crit. Rev. Biochem.* **19,** 191–245
46. Spolar, R.S., Record, M. T., Jr. (1994) Coupling of local folding to site-specific binding of proteins to DNA. *Science* **263,** 777–784
47. Sturtevant, J. M. (1977) Heat capacity and entropy changes in processes involving proteins. *Proc. Natl. Acad. Sci. U.S.A.* **74,** 2236–2240
48. Cooper, A., Johnson, C. M., Lakey, J. H., and Nöllmann, M. (2001) Heat does not come in different colours: entropy-enthalpy compensations, free energy windows, quantum confinement, pressure perturbation calorimetry, solvation and the multiple causes of heat capacity effects in biomolecular interactions. *Biophys. Chem.* **93,** 215–230